CHAPTER I

INTRODUCTION

For the foreseenable future, liquid hydrocarbon fuels will play a significant role in the transportation sector of the world. Factors favoring these fuels include convenience, high energy density, and the vast existing infrastructure for their production and use. A scenario and time frame are developed in which declining world resources will generate a shortage in petroleum supply that can be alleviated in part by utilizing the abundant coal resource base. One option is direct or indirect coal conversion to liquid transportation fuels.

Coal can be converted into liquid fuels by liquefaction process. One important route for indirect liquefaction is hydrogenation of carbon monoxide which yield methanol at high yields. Methanol is suitable for direct use as a turbine and transportation fuel, although its energy content on a volume basis is only half that of gasoline. It can also be used as a feedstock to produce high octane gasoline.

For methanol production technologies, considerable research and development still need to be undertaken. To produce liquid phase methanol products, several reactor systems such as fixed bed reactor, entrained bed reactor, fixed fluidized bed reactor and slurry bubble column reactor, have been developed. Among these reactor systems, the three-phase slurry bubble column reactors provide an attractive alternative to the others since they can be operated with low H_2/CO ratio (<0.6) synthesis gas.

The Air Products and Chemicals (1987) had developed a methanol synthesis technology with the slurry bubble column reactor at its LaPorte Pilot Plant since the early

80's. The liquid phase methanol was obtained during a number of test runs with variety conditions.

To test high catalyst concentration using a commercial synthesis catalyst with CO-rich gas and to evaluate the short-term activity of a commercial catalyst with CO-rich gas, a series of runs was conducted (Air Products 1987). These runs suggested that the hydrodynamics of the slurry bubble reactor with high-catalyst slurry concentration needs to be studied further.

The objective of this study is to improve the hydrodynamics understanding on the slurry bubble column reactors using IIT's hydrodynamic models and computer code.

The IIT's hydrodynamic code, original developed from the K-FIX program (Rivard and Torrey, 1977), was able to predict a great deal of the behaviors of bubbling beds (Gidaspow and Ettehadieh 1983a, Gidaspow et al. 1983b, Ettehadieh 1982, Syamlal 1985, and Gidaspow et al. 1985 and Gamwo 1992), circulating fluidized bed (Therdthianwong 1994 and Ding 1990) and gas-liquid-solid three-phase fluidized bed (Jayaswal 1991 and Bahary 1994). Gidaspow's book (Gidaspow 1994), "Multiphase Flow and Fluidization, Continuum and Kinetic Theory Descriptions," detail describes these fundamental approaches of IIT's hydrodynamic models. His kinetic theory had been programmed to the code to compute the particulate viscosities and solids pressure (Ding and Gidaspow 1990; Gidaspow et al. 1991).

To simulate the slurry bubble column reactors, the IIT's code has been modified properly to satisfied particular needs in this study. For instance, modules for chemical reactions (particular for the synthesis of methanol), phase changes and heat exchangers were added to the code. Also the kinetic theory was used to compute the viscosity of the

catalyst. The models and governing equations of the hydrodynamics, chemical kinetics, heat and mass transfers are described in Chapter II.

To investigate the effects of gas and liquid superficial velocities, operation temperature and pressure on the gas hold-up, a number of simulation runs for gas hold-up were made. Chapter III describes these gas hold-up runs. The gas hold-ups are very close to those measurements obtained from the Air Products' (1987) pilot plant.

Air Products' (1987) RUN E-2 series were the operations of liquid phase methanol with the external slurry circulation. In this study, a dynamic simulation for the RUN E-2-B was conducted. As described in Chapter IV, the computed time-and-cross-section-area-averaged catalyst concentration profiles match well with Air Products' NDG (Nuclear Density Gauge) measurements.

Air Products' (1991) RUN E-8 series were the operations of liquid phase methanol without the external slurry circulation. In this study, a dynamic simulation for the RUN E-8.1 was conducted. The kinetic theory had been used to compute the catalyst viscosities and energy equation had been solved to predict the temperature profiles in count of the internal heat exchangers. As described in Chapter V, the slurry height, methanol production and gas-liquid-solid volume fraction profiles agreed well with that obtained at the Air Products' (1991) pilot plant. A simulation with a finer grid was carried out to investigate the effect of grid on the accuracy and convergence of the numerical computation.

As part of this thesis research, a series of simulations for the coal-pyrite separation in an inclined electro-fluidized bed was performed. Chapter VI describes the results of these simulations. The kinetic theory had been applied to predict the viscosities for both

solids, coal and pyrite. The study had achieved that the pyrite can be removed in a great deal from coal in an inclined electro-fluidized bed.

In Appendix A, a description of governing hydrodynamic equations, the finite difference equations and the solution techniques are presented. Appendix B describes a detail user menu for the multiple functional code, MFREK, which stands Multiphase Flow with Reactions, Energy equations and Kinetic theory. Appendix C lists the source FORTRAN code of MFREK.

CHAPTER II

DESCRIPTIONS OF HYDRODYNAMIC MODELS

2.1 Introduction

The hydrodynamic approach to multiphase flow systems is based on the principles of mass conservation, momentum balance and energy conservation for each phase. This approach is similar to that of Soo (1967) for multiphase flow and of Jackson (1985) for fluidization. Gidaspow (1986), recently reviewed such models as they apply to fluidization and analyzed the necessary steps required to ensure that momentum equations satisfy the Darcy's law and Archimedes' principles.

A transient, two-dimensional hydrodynamic models for multiphase flow of fluid and particulate phases based on the generalization of Navier-Stokes equations was developed at IIT. The review by Gidaspow (1986) showed that inviscid two-fluid models were able to predict a great deal of the behavior of bubbling beds because the dominant mechanism of energy dissipation is the drag between the particles and the fluid. Ding and Gidaspow (1990) extended the model to include solids viscosity from kinetic theory of granular flows and used it to predict the behavior of bubbling beds. The present model has been extended the kinetic theory to gas-liquid-solid fluidized beds and gas-solid-solid binary systems. Besides, a general model for chemical and mass transfer between phases has been developed.

2.2 Hydrodynamic Models

The hydrodynamic models for gas-liquid-solid or gas-solid-solid binary system with phase changes are described as followings.

2.2.1 Continuity Equations. The conservation of mass can be interpreted as that:

rate of mass accumulation + convection due to flow = production due to mass transfer.

Gas Phase:

$$\frac{\partial}{\partial t}(\varepsilon_g \rho_g)+\nabla\cdot(\varepsilon_g \rho_g \mathbf{v}_g)=\dot{m}_g$$

Liquid and Solid phases: ($\mathbf{k}=\ell,\mathbf{s}$)

$$\frac{\partial}{\partial t}(\varepsilon_k \rho_k)+\nabla\cdot(\varepsilon_k \rho_k \mathbf{v}_k)=\dot{m}_k$$

In above equations, the volume fractions of each phase must be added up to unity, and they can be related by

$$\varepsilon_g+\varepsilon_\ell+\varepsilon_s=1$$

2.2.2 Momentum Equations. The momentum equation for each phase can be interpreted as Newton's first law:

mass x acceleration = sum of forces acting on the phase.

As described in Chapter 2 of the book by Gidaspow (1994), there are three different types of momentum balances, model A, model B and model C. In model A, the pressure drop occurs in each involving phase. An alternative way to treat the pressure drop is to assume that it occurs only in the gas phase or the continuous phase. This is called as model B (Gidaspow 1977, Arastoopour and Gidaspow 1979). Model C is similar to model B except of the solid velocity which is replaced with the relative velocity (v_s-v_g). Lyczkowski et al. (1978) had found that the momentum equations with model B is well-posed and possesses all real characteristics.

Gas Phase:

$$\frac{\partial}{\partial t}(\varepsilon_g \rho_g v_g)+\nabla\cdot(\varepsilon_g \rho_g v_g v_g)=\varepsilon_g \rho_g F_g+\sum_{m=\ell,s}\beta_{gm}(v_m-v_g)+\nabla\cdot[\tau_g]+\dot{m}_g v_g$$

Liquid and Solid Phases: ($k=\ell,s$)

$$\frac{\partial}{\partial t}(\varepsilon_k \rho_k v_k)+\nabla\cdot(\varepsilon_k \rho_k v_k v_k)=\varepsilon_k \rho_k F_k+\sum_{m=g,\ell,s}\beta_{km}(v_m-v_k)+\nabla\cdot[\tau_k]+\dot{m}_k v_k$$

2.2.3 Energy Equations. To treat non-isothermal multiphase flow systems, the energy equations are needed to compute the heat transfer due to heat exchangers and chemical reactions. The equations are written based on the principle of thermodynamics first law:

rate of energy accumulation = heat received - work done by the system

Gas Phase:

$$\frac{\partial}{\partial t}(\varepsilon_g \rho_g H_g)+\nabla\cdot(\varepsilon_g \rho_g H_g v_g)=(\frac{\partial P_g}{\partial t}+P_g \nabla\cdot v_g)+\nabla\cdot(k_g \nabla T_g)+\Phi_g+\sum_i r_{ig}\Delta H_{ig}$$
$$+\sum_{m=\ell,s}\left\{h_{vm}(T_m-T_g)+\beta_{gm}(v_m-v_g)^2-\dot{m}_m H_g\right\}$$

Liquid and Solid Phases: ($k=\ell,s$)

$$\frac{\partial}{\partial t}(\varepsilon_k \rho_k H_k)+\nabla\cdot(\varepsilon_k \rho_k H_k v_k)=h_{vk}(T_g-T_k)+\sum_{m=g,\ell,s}\beta_{km}(v_m-v_k)^2+\dot{m}_k H_g$$
$$+\nabla\cdot(k_k \nabla T_k)+\sum_i r_{ik}\Delta H_{ik}+\Phi_k$$

2.3 Constitutive Equations

In order to solve the set of conservation equations of mass, momentum and energy, all the constitutive equations must be defined.

2.3.1 Equation of State. The gas phase is compressible fluid and obeys the equation of state.

$$\rho_g = \frac{\overline{M}_g P_g}{zRT_g}$$

2.3.2 Drag Coefficients. The drag coefficients for model B are based on Ergun equation and empirical correction depending on the gas porosity.

$$\beta_{gk} = \beta_{kg} = 150\frac{(1-\varepsilon_g)\varepsilon_k \mu_g}{(\varepsilon_g d_k \psi_k)^2} + 1.75\frac{\rho_g \varepsilon_k |v_g - v_k|}{\varepsilon_g d_k \psi_k} \qquad \varepsilon_g > 0.8$$

$$\beta_{gk} = \beta_{kg} = \frac{3}{4} C_D \frac{\rho_g \varepsilon_k |v_g - v_k|}{d_k \psi_k} \varepsilon_g^{-2.65} \qquad \varepsilon_g < 0.8$$

where

$$C_D = \frac{24}{Re_k}(1 + 0.15 Re_k^{0.687})$$

$$Re_k = \frac{\rho_g \varepsilon_g |v_g - v_k| d_k \psi_k}{\mu_g} \qquad Re_k = 1000 \quad \text{if} \quad Re_k > 1000$$

$$\beta_{\ell s} = \beta_{s\ell} = \frac{3}{2}(1+e)\frac{\rho_s \rho_\ell \varepsilon_s \varepsilon_s |v_\ell - v_s|}{\rho_s d_s^3 + \rho_\ell d_\ell^3}(d_s + d_\ell)^2$$

2.3.3 External Forces Acting on Each Phase. The external forces acting on each phase consist of the gravity, electric or magnetic force if applied, etc.

$$F_g = \frac{g}{\varepsilon_g}$$

$$F_k = \frac{g}{\varepsilon_g}\left(1 - \frac{1}{\rho_k}\sum_{m=g,\ell,s} \varepsilon_m \rho_m\right) + q_k E \qquad k = \ell, s$$

The q_k is the particle surface charge and the E is the strength of electric field applied.

2.3.4 Shear Stresses. The gas is considered as a Newtonian fluid. The solid shear stress consists of the solid press (P_k), cohesive force (τ_{ck}), and shear rate due to solid shear viscosity (μ_k) and solid phase bulk viscosity (ξ_k).

$$[\tau_g]=\left\{-P_g-\frac{2}{3}\mu_g\varepsilon_g\nabla\cdot v_g\right\}[I]+\mu_g\varepsilon_g\left[\nabla v_g+(\nabla v_g)^T\right]$$

$$[\tau_k]=\left\{-P_k+\tau_{ck}+(\xi_k-\frac{2}{3}\mu_k)\nabla\cdot v_k\right\}[I]+\mu_k\left[\nabla v_k+(\nabla v_k)^T\right] \qquad k=\ell,s$$

The empirical cohesive force can be given:

$$\tau_{ck}=10^{10.6\varepsilon_k+5.5} \qquad k=\ell,s$$

The solid pressure and viscosities expressions from kinetic theory will be described in section 2.4 of this chapter. Here lists some empirical correlations. ($k=\ell,s$)

$$\mu_k=5\varepsilon_k \qquad \xi_k=0$$

$$\nabla P_k=G(\varepsilon_k)\nabla\varepsilon_k \qquad G(\varepsilon_k)=10^{8.76\varepsilon_k-0.27}$$

2.3.5 Enthalpy

$$H_g=C_{p_g}(T_g-T_g^0)$$

$$H_k=C_{p_k}(T_k-T_k^0)$$

2.3.6 Gas-Solid Heat Transfer. (Gunn's Model)

$$Nu_k=\left\{(2+5\varepsilon_k^2)(1+0.7Re_k^{0.2}Pr^{1/3})+(\frac{2}{15}+1.2\varepsilon_k^2)Re_k^{0.7}Pr^{1/3}\right\}Sp_k$$

$$Nu_k=\frac{h_{vk}d_k}{k_g^0} \qquad Pr=\frac{C_{p_g}\mu_g}{k_g^0} \qquad Sp_k=\frac{6\varepsilon_k}{d_k}$$

2.3.7 Gas Phase Heat Transfer

$$k_g^0=8.65\times10^5\left(\frac{T_g}{1400}\right)^{1.786}$$

$$k_g=(1-\sqrt{1-\varepsilon_g})k_g^0$$

2.3.8 Particulate Phase Heat Transfer

$$\frac{k_k}{k_g^0}=\frac{\sqrt{\varepsilon_s}}{(1-\varepsilon_g)}\left\{\varphi\frac{k_k^*}{k_g^0}+(1-\varphi)\frac{k_k^0}{k_g^0}\right\}$$

$$\frac{k_k^0}{k_g^0}=\frac{2}{A_k}\left\{\frac{B_k\left\{(k_k^*/k_g^0)-1\right\}}{A_k^2(k_k^*/k_g^0)}\cdot\ln\frac{(k_k^*/k_g^0)}{B_k}\frac{B_k-1}{A_k}\frac{B_k+1}{2}\right\}$$

where

$$A_k=1-\frac{B_k}{(k_k^*/k_g^0)}$$

$$B_k=1.25\left(\frac{\varepsilon_k}{\varepsilon_g}\right)^{10/9}(1+3\chi)$$

$$\chi=\sqrt{\frac{\left(\sum\varepsilon_k\rho_k\right)\left(\sum\varepsilon_k\rho_k/d_k^2\right)}{\left(\sum\varepsilon_k\rho_k/d_k\right)^2}-1}\qquad k=l,s$$

$$k_k^*=0.3289\qquad \varphi=7.26\times10^{-3}$$

2.4 Solid Viscosity from Kinetic Theory Approach

The solid viscosity or solid shear stresses of multiphase flow may not be constant or as a function of the solid concentration in the rapid shear flow regime. Experiments of Savage and Sayed (1984) have shown that the solid stress is proportional to the square of the shear rate in a certain range of shear rate of simple shear flows. To model the solid shear stress, the statistical approach may be used to formulate the constitutive equations for the solid phase. Analogous to those used in the kinetic theory of dense gases (Chapman and Cowling 1970), several models for the flow of granular materials have been developed based on the assumptions that the collisions between the particles provide the principal mechanism for the transport properties, such as momentum and energy, and that

the velocity distribution function of single-particle is Maxwellian (Savage and Jeffery 1981, Jenkins and Savage 1983). Savage (1983) and Jenkins and Savage (1983) have developed the kinetic theory approach by introducing the concept of restitutive coefficient and by using the Boltzmann transport equation for dense gases. Ding and Gidaspow (1990) extended their approach to particle flow for dense phase. In this study, the kinetic theory approach has been applied to gas-liquid-solid three phase fluidization and gas-solid-solid binary systems.

Fluctuating Energy Equation. ($k=\ell,s$)

$$\frac{3}{2}\left[\frac{\partial}{\partial t}(\varepsilon_k\rho_k\Theta_k)+\nabla\cdot(\varepsilon_k\rho_k\Theta_k v_k)\right]=\nabla\cdot(\kappa_k\nabla\Theta_k)-\gamma_k-3\beta_{kg}\Theta_k+\Phi_k$$

Energy Production Rate

$$\Phi_k=[\tau_k]:\nabla v_k \qquad k=g,\ell,s$$

Conductive Coefficient of Fluctuating Energy.

$$\kappa_k=\frac{2\kappa_{k_{dil}}}{(1+e_k)g_{0k}}\left\{1+\frac{6}{5}(1+e_k)g_{0k}\varepsilon_k\right\}^2+2\varepsilon_k^2\rho_k d_k g_{0k}(1+e_k)\sqrt{\frac{\Theta_k}{\pi}}$$

Collisional Energy Dissipation.

$$\gamma_k=3(1-e_k^2)\varepsilon_k^2\rho_k g_{0k}\Theta_k\left\{\frac{4\sqrt{\Theta_k}}{d_k\sqrt{\pi}}-\nabla\cdot v_k\right\}$$

Solids Pressure.

$$P_k=\rho_k\varepsilon_k\Theta_k\{1+2(1+e_k)g_{0k}\varepsilon_k\}$$

Solids Bulk Viscosity.

$$\xi_k=\frac{4}{3}\varepsilon_k^2\rho_k d_k g_{0k}(1+e_k)\sqrt{\frac{\Theta_k}{\pi}}$$

Solids Shear Viscosity.

$$\mu_k = \frac{2\mu_{k_{dil}}}{(1+e_k)g_{0k}}\left\{1+\frac{4}{5}(1+e_k)g_{0k}\varepsilon_s\right\}^2 + \frac{4}{5}\varepsilon_k^2\rho_k d_k g_{0k}(1+e_k)\sqrt{\frac{\Theta_k}{\pi}}$$

Where

$$g_{0k} = \left\{1-\left(\frac{\varepsilon_k}{\varepsilon_{k_{max}}}\right)^{1/3}\right\}^{-1} \qquad \mu_{k_{dil}} = \frac{5}{96}\rho_k d_k\sqrt{\pi\Theta_k} \qquad \kappa_{k_{dil}} = \frac{75}{384}\rho_k d_k\sqrt{\pi\Theta_k}$$

2.5 Reaction and Mass Transfer

General Reactions

$$\sum_j^N \alpha_{ik}^j S^j = 0 \qquad i=1,2,\cdots,M_k \qquad k=g,\ell,s$$

where S^j represents the jth specie and α_{ik}^j represents the stoichiometric coefficient of the jth specie in the ith reaction of phase k.

$$r_{ik} = f_{ik}(P_k, T_k, \varepsilon_k, y_k^1, y_k^2, \cdots, y_k^N, \cdots) \qquad i=1,2,\cdots,M_k \quad k=g,\ell,s$$

The overall rate r_{ik} may be a function of temperature, pressure, catalyst concentration and compositions.

Mass Transfer Between Phases

$$R_k^j = f_k^j(P_k, T_k, a_k, y_k^1, y_k^2, \cdots, y_k^N, P_g, T_g, y_g^1, y_g^2, \cdots, y_g^N, \cdots) \qquad k=\ell,s$$

The mass transfer rate R_k^j of the jth specie between the phase k and the continuous phase (gas) may be a function of temperature, pressure, interfacial area and compositions.

2.6 Species Balances (j=1, 2, ..., N)

Gas Phase:

$$\frac{\partial}{\partial t}(\varepsilon_g \rho_g y_g^j)+\nabla\cdot(\varepsilon_g \rho_g y_g^j v_g)=\sum_{i=1}^{M_g}\alpha_{ig}^j M^j r_{ig}-\sum_{k=\ell,s} M^j R_k^j$$

Liquid and Solid Phases: ($k=\ell,s$)

$$\frac{\partial}{\partial t}(\varepsilon_k \rho_k y_k^j)+\nabla\cdot(\varepsilon_k \rho_k y_k^j v_k)=\sum_{i=1}^{M_k}\alpha_{ik}^j M^j r_{ik}+M^j R_k^j$$

$$\sum_{j}^{N} y_k^j=1 \qquad k=g,\ell,s$$

Phase Changes: ($k=\ell,s$)

$$\dot{m}_k=\sum_{j}^{N} M^j R_k^j \qquad \dot{m}_g=-\sum_{k=\ell,s}\dot{m}_k$$

CHAPTER III

GAS HOLD-UP OF GAS-LIQUID FLUIDIZATION

3.1 Introduction

The gas holdup in slurry bubble columns is affected by a number of factors which include: physical properties and coalescing behavior of liquid, gas and liquid velocities, column diameter, gas distributor design. The gas holdup also depends on the operating flow regime in the column. The development of a general correction which takes into account the effect of all these variables is indeed a difficult task.

According to the traditional opinion, gas and liquid velocities have most significant effect on gas holdup. Recent studies, however, show that gas holdup in bubble columns generally increases with increasing operating pressure, hence gas density (Idogawa et al. 1987, Clark 1990 and Kojinma et al. 1991). The influence of pressure has been found to depend on pressure level, distributor type, gas and liquid velocities. These results show that a correlation for gas holdup should account for the effect of operating pressure (or gas density) too. Most of the literature correlations, however, is based on data obtained at atmospheric pressure and usually for one gas, as a result these equations do not account for any influence of gas density. A few gas holdup equations have been developed based on high pressure operation (Idogawa et al. 1986 and 1987) or experiments using various gases (Reilly et al. 1986 and Hammer et al. 1984). There is, however, a lack of systematic research to investigate the influence of pressure on gas holdup in slurry bubble columns. Correlations for gas holdup in slurry bubble columns have been proposed by a number of researchers including Deckwer et al. (1980), Koide et al. (1984), Sada et al. (1986), Sauer

and Hempel (1987) and Bukur et al. (1990). These experimental correlations can not take into account the effect of pressure, temperature, gas and liquid velocities. In this chapter, hydrodynamic models for gas holdup are developed and used to predict the gas holdup of LaPorte's RUN E-3 series (Air Products 1987).

3.2 Hydrodynamic Models

The hydrodynamic models employed in the simulations of gas-liquid fluidization are based on the principle of conservations of mass and momentum for both gas and liquid phases (Gidaspow 1994). No energy equation is needed because of an isothermal assumption. Gas is treated as continuous phase while liquid as disperse phase. The governing equations are expressed as following:

3.2.1 Conservation of Mass

Gas Phase.

$$\frac{\partial}{\partial t}(\varepsilon_g \rho_g)+\nabla\cdot(\varepsilon_g \rho_g \mathbf{v}_g)=0$$

Liquid Phase.

$$\frac{\partial}{\partial t}(\varepsilon_k \rho_k)+\nabla\cdot(\varepsilon_k \rho_k \mathbf{v}_k)=0$$

3.2.2 Conservation of Momentum

Gas Phase.

$$\frac{\partial}{\partial t}(\varepsilon_g \rho_g \mathbf{v}_g)+\nabla\cdot(\varepsilon_g \rho_g \mathbf{v}_g \mathbf{v}_g)=\varepsilon_g \rho_g \mathbf{F}_g+\beta_{gk}(\mathbf{v}_k-\mathbf{v}_g)+\nabla\cdot[\tau_g]$$

Liquid Phase.

$$\frac{\partial}{\partial t}(\varepsilon_k \rho_k \mathbf{v}_k)+\nabla\cdot(\varepsilon_k \rho_k \mathbf{v}_k \mathbf{v}_k)=\varepsilon_k \rho_k \mathbf{F}_k+\beta_{kg}(\mathbf{v}_g-\mathbf{v}_k)+\nabla\cdot[\tau_k]$$

3.2.3 Constitutive Equations

$$\varepsilon_g+\varepsilon_\ell=1$$

Equation of State:

$$\rho_g=\frac{\overline{M}_g P_g}{zRT_g}$$

Drag Coefficients: (Based on Ergun Equation)

$$\beta_{gk}=\beta_{kg}=150\frac{(1-\varepsilon_g)\varepsilon_k\mu_g}{(\varepsilon_g d_k\psi_k)^2}+1.75\frac{\rho_g\varepsilon_k|v_g-v_k|}{\varepsilon_g d_k\psi_k} \qquad \varepsilon_g>0.8$$

$$\beta_{gk}=\beta_{kg}=\frac{3}{4}C_D\frac{\rho_g\varepsilon_k|v_g-v_k|}{d_k\psi_k}\varepsilon_g^{-2.65} \qquad \varepsilon_g<0.8$$

where

$$C_D=\frac{24}{Re_k}(1+0.15Re_k^{0.687})$$

$$Re_k=\frac{\rho_g\varepsilon_g|v_g-v_k|d_k\psi_k}{\mu_g} \qquad Re_k=1000 \quad \text{if} \quad Re_k>1000$$

External Forces Acting on Each Phase.

$$F_g=\frac{g}{\varepsilon_g}$$

$$F_k=\frac{g}{\varepsilon_g}\left(1-\frac{1}{\rho_k}\sum_{m=g,k}\varepsilon_m\rho_m\right)$$

Shear Stresses.

$$[\tau_g]=\left\{-P_g-\frac{2}{3}\mu_g\varepsilon_g\nabla\cdot v_g\right\}[I]+\mu_g\varepsilon_g\left[\nabla v_g+(\nabla v_g)^T\right]$$

$$[\tau_k]=\left\{-P_k+\tau_{ck}+\left(\xi_k-\frac{2}{3}\mu_k\right)\nabla\cdot v_k\right\}[I]+\mu_k\left[\nabla v_k+(\nabla v_k)^T\right]$$

Cohesive Force.

$\tau_{ck}=10^{10.6\varepsilon_k+5.5}$

Empirical stress modules.

$\mu_k=5\varepsilon_k$ $\xi_k=0$

$\nabla P_k=G(\varepsilon_k)\nabla\varepsilon_k$ $G(\varepsilon_k)=10^{8.76\varepsilon_k-0.27}$

3.3 Operating Conditions

The operating conditions, which cover a wide range of temperature, pressure, gas and liquid velocities, are chosen from the gas-liquid two-phase RUN E-3 series at LaPorte pilot plant (Air Products 1987).

Diameter of the reactor	59 cm
Height of the reactor	600 cm
Superficial gas velocity	0--20 cm/s
Superficial liquid velocity	0--12 cm/s
Temperature	76--250 °C
Pressure	170--6,310 kPa
Gas	N_2
Liquid	Freeze-100
Density of liquid	0.861-0.000643xT (°C)
Number of cells in the grid	34x33
Time interval	10^{-4} sec.

3.4 Numerical Considerations

3.4.1 Initial Conditions. The initial gas hold-up and velocities are assumed to be uniform over the whole bed. A constant pressure, listed in Table 3.1, is kept at the top of the bed and isothermal is assumed in these simulation runs. The initial conditions are summerized as following:

gas	liquid
$\varepsilon_g=0.1$	$\varepsilon_\ell=0.9$
$u_g=0$	$u_\ell=0$
$v_g=1cm/s$	$v_\ell=0$
$T_g=T_0$	$T_\ell=T_0$
$P_g=P_0$	$P_\ell=P_0$

3.4.2 Boundary Conditions. The inflow conditions, including gas and liquid velocities and volume fractions, and the top pressure are prescribed. Assumption of non-slip at the walls is made for both gas and liquid phases. The boundary conditions around the computing mesh, shown as Figure 3.1, are summerized as following.

Table 3.1 Computed and Measured Gas Holdups at Reactor Height 137cm

Test #	P (kPa)	T °C	V_g cm/s	V_l m/s	ε_g (test)	ε_g (computed)	Error %
E-3-4	170	76	4	2	0.1300	0.1430	10.0
E-3-5	170	76	7	2	0.2000	0.1950	-2.5
E-3-6	170	76	13	2	0.2800	0.3030	8.2
E-3-7	170	76	20	2	0.3200	0.2789	-12.8
E-3-8	660	76	3	2	0.1800	0.1694	-5.9
E-3-9	660	76	7	2	0.2600	0.2483	-4.5
E-3-13	6310	76	3	2	0.2400	0.2403	0.1
E-3-14	6310	76	6	2	0.3800	0.3607	-5.1
E-3-15	6310	76	8	2	0.4200	0.3983	-5.2
E-3-16	6310	149	12	2	0.4900	0.4633	-5.4
E-3-17	6310	149	10	2	0.4400	0.4197	-4.6
E-3-18	6250	153	4	2	0.2500	0.2361	-5.6
E-3-20	6340	224	3	2	0.1900	0.2133	12.3
E-3-21	6310	226	6	2	0.3400	0.3820	12.4
E-3-22	6310	223	8	2	0.4500	0.5220	16.0
E-3-23	6310	221	11	2	0.4900	0.6165	25.8
E-3-28	660	77	12	2	0.3200	0.3070	-4.1
E-3-29	660	77	19	2	0.3800	0.4170	9.7
E-3-35	6310	149	10	2	0.4600	0.4825	18.1
E-3-36	6310	149	9	5	0.4300	0.4122	-4.1

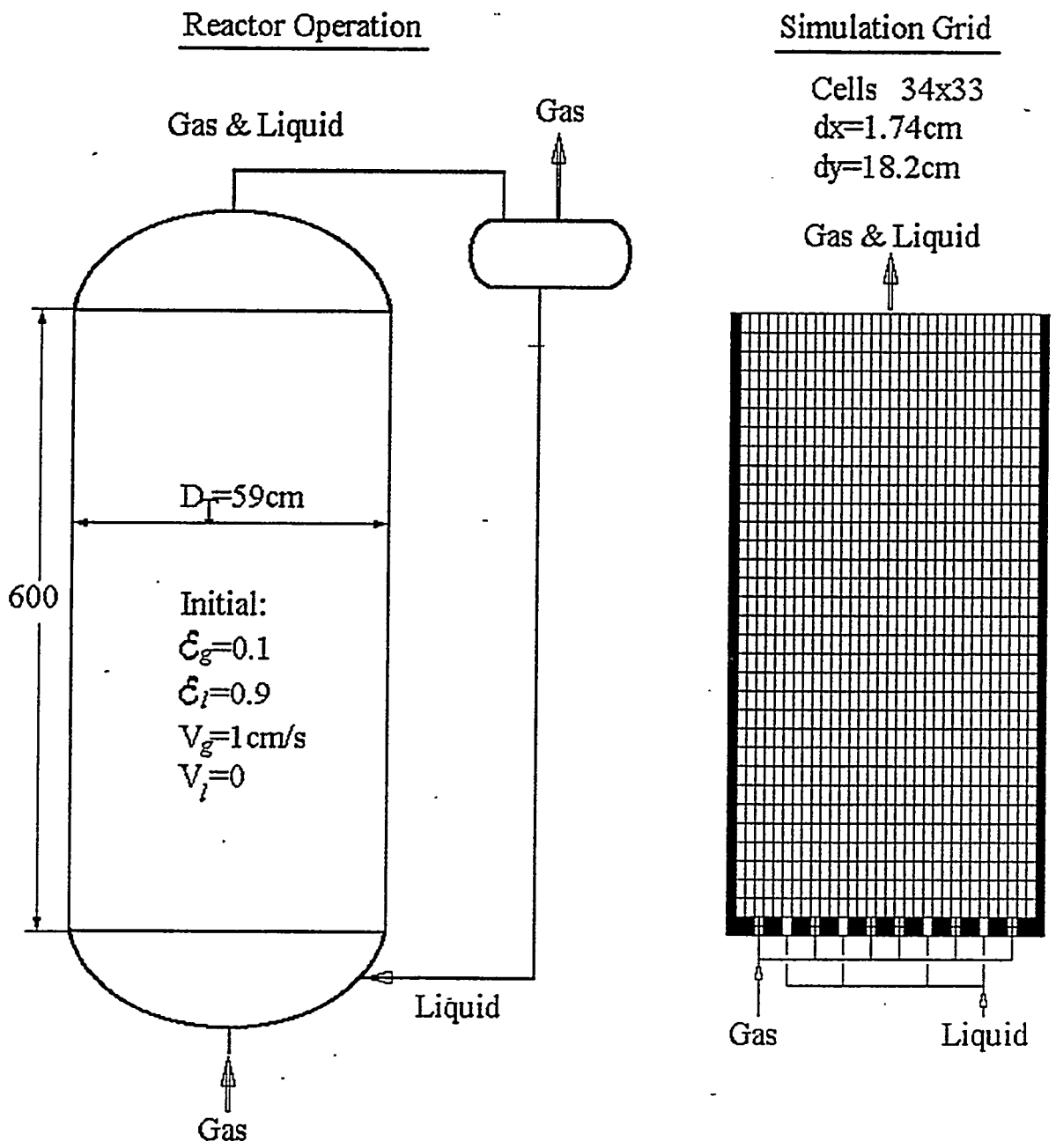

Figure 3.1 Reactor Operation and Simulation Grid

		gas	liquid
bottom	**gas orifice**	$\varepsilon_g=1$	$\varepsilon_\ell=0$
		$v_g=v_{g0}$	$v_\ell=0$
		$u_g=0$	$u_\ell=0$
	liquid orifice	$\varepsilon_g=0$	$\varepsilon_\ell=1$
		$v_g=0$	$v_\ell=v_{\ell 0}$
		$u_g=0$	$u_\ell=0$
	wall	$v_g=0$	$v_\ell=0$
		$u_g=0$	$u_\ell=0$
left/right		$v_g=0$	$v_\ell=0$
		$u_g=0$	$u_\ell=0$
top		$\frac{\partial \varepsilon_g}{\partial y}=0$	$\frac{\partial \varepsilon_\ell}{\partial y}=0$
		$\frac{\partial v_g}{\partial y}=0$	$\frac{\partial v_\ell}{\partial y}=0$
		$u_g=0$	$u_\ell=0$
		$P_g=P_0$	$P_\ell=P_0$

3.5 Results and Discussions

The computing time for each case listed on Table 3.1 is 20 seconds and the gas holdup is time and cross section area average value.

The axial gas holdup profiles at various superficial gas velocities are shown in Figure 3.2. Both measured at Air Products' pilot plant and computed gas hold-up profiles exhibit the trend toward higher gas volume fraction at higher elevations, specially at high superficial gas velocity. There are about 20% differences between the simulations and measurements around the lower elevations at high superficial gas velocities, because of the

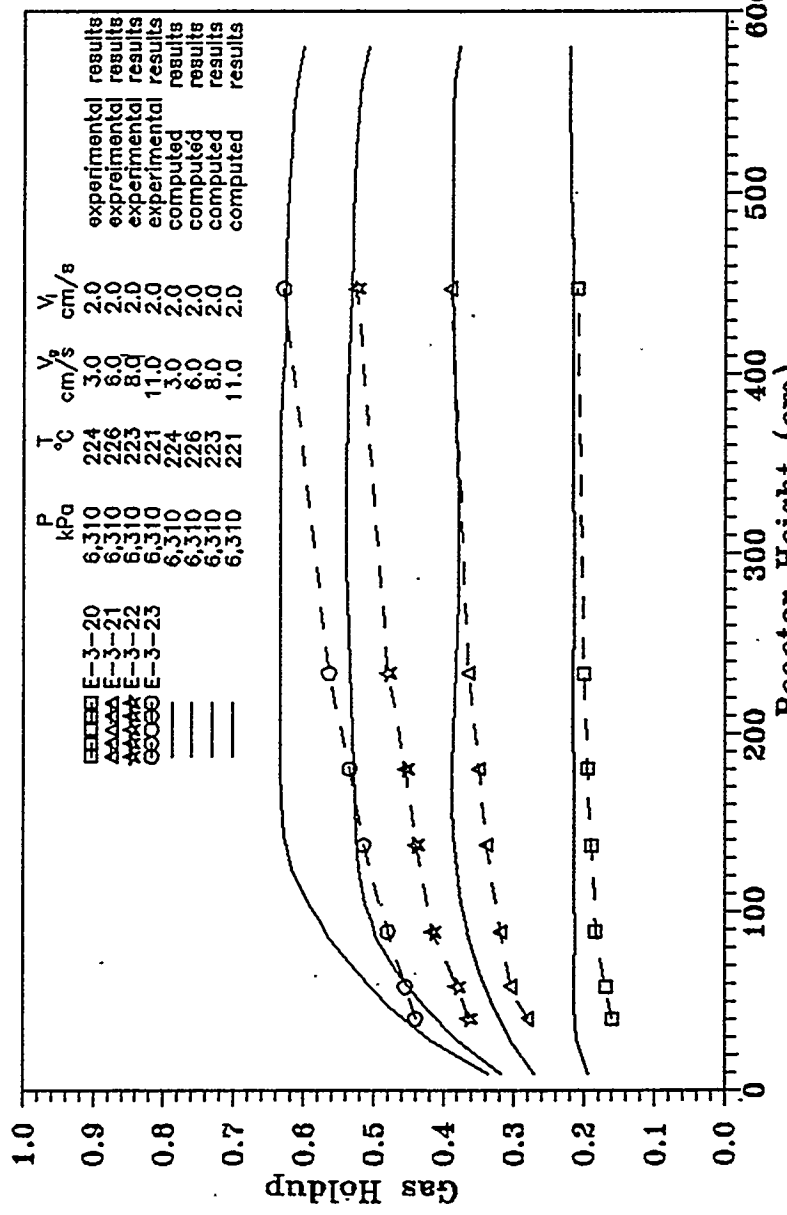

Figure 3.2 Computed and Experimental Gas Holdup Profiles

significant wall effect at high gas velocity. Figure 3.2 shows that gas hold-up increases with the increasing in gas velocity also.

Figure 3.3 shows the effects of liquid velocity on the gas hold-up. Two liquid velocities, 2 cm/s and 5 cm/s were used in the simulations. The gas hold-up at higher liquid velocity is slightly less than that of the lower liquid velocity because of the introduction of more liquid. The slopes of curves in Figure 3.3 indicate a longer entrance length occurring at high liquid velocity.

As shown in Figure 3.4, the superficial gas velocity has a significant and positive effect on the gas hold-up.

Temperature has little effect on the gas hold-up since the temperature does not change the gas density as much as the pressure does (Figure 3.5).

Figure 3.6 shows the effect of pressure on gas hold-up. High gas hold-up has been observed with high pressure because the gas density is sensitive to the pressure. It is seem that high pressure compresses from leaving the system.

The measured and computed gas hold-ups at the reactor's elevation 137 cm from its bottom are listed in Table 3.1. Compared with measurements, the computed results have an error lying in 0--25% (see Figure 3.7).

In summary, the gas hold-ups, computed with a variety of operating conditions such as temperature, pressure, gas and liquid velocities, agree well with the measurements obtained at Air Products' pilot plant. The hydrodynamic model has more flexible features than those empirical correlations in predicting the gas hold-up of gas-liquid two-phase flow systems.

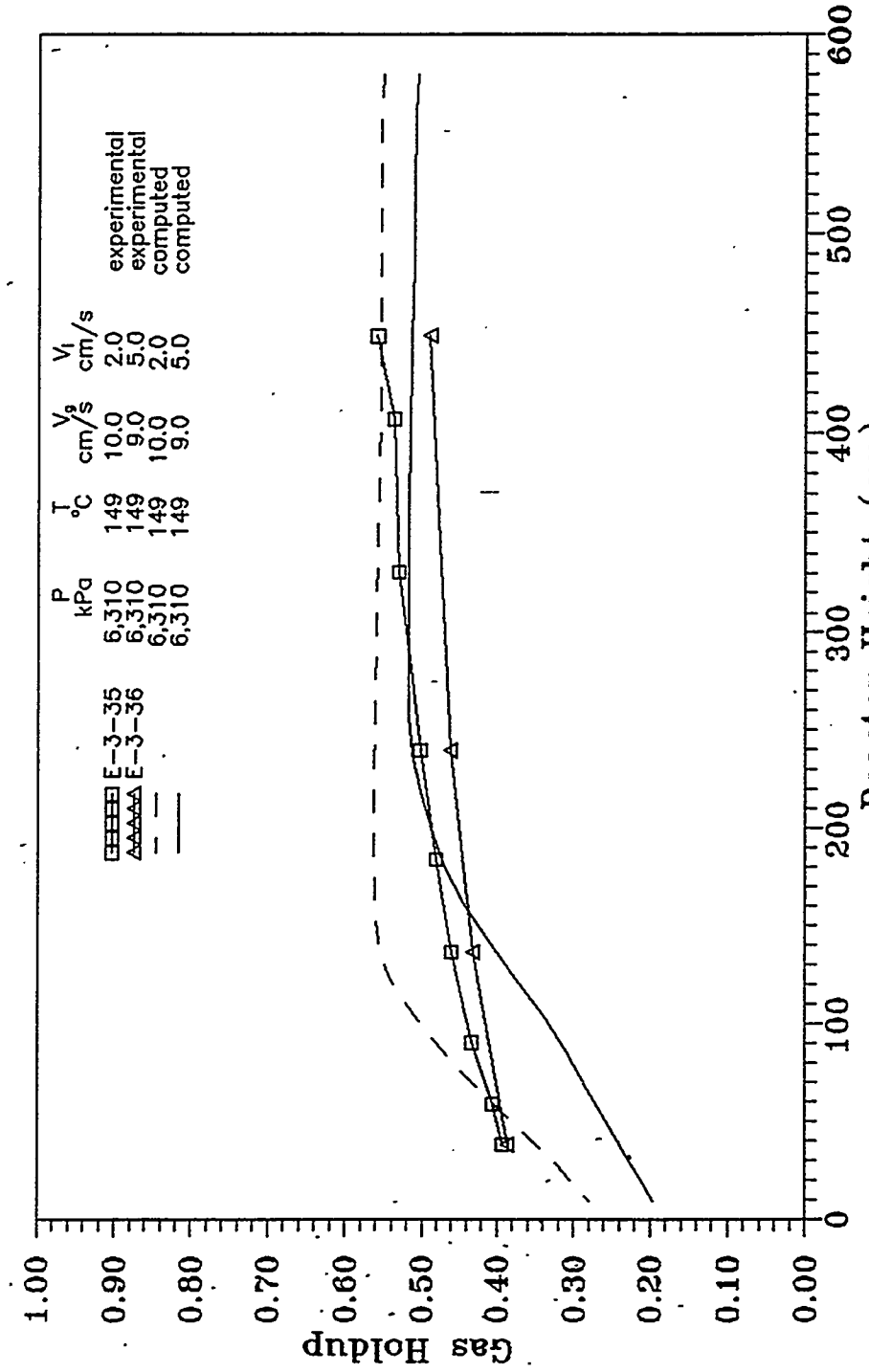

Figure 3.3 Computed and Experimental Axial Gas Holdup Profiles(Effect of Liquid Velocity)

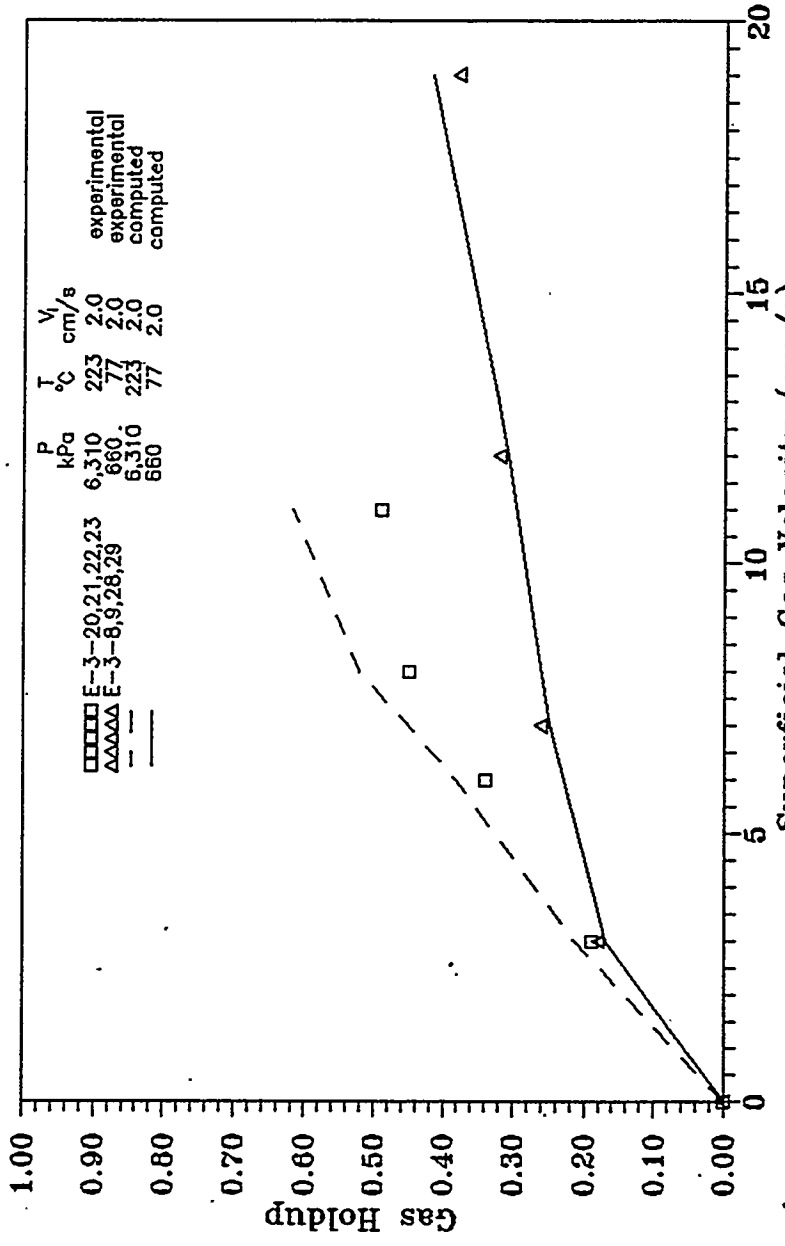

Figure 3.4 Computed and Experimental Gas Holdup vs Gas Velocity (at Reactor Height=137cm)

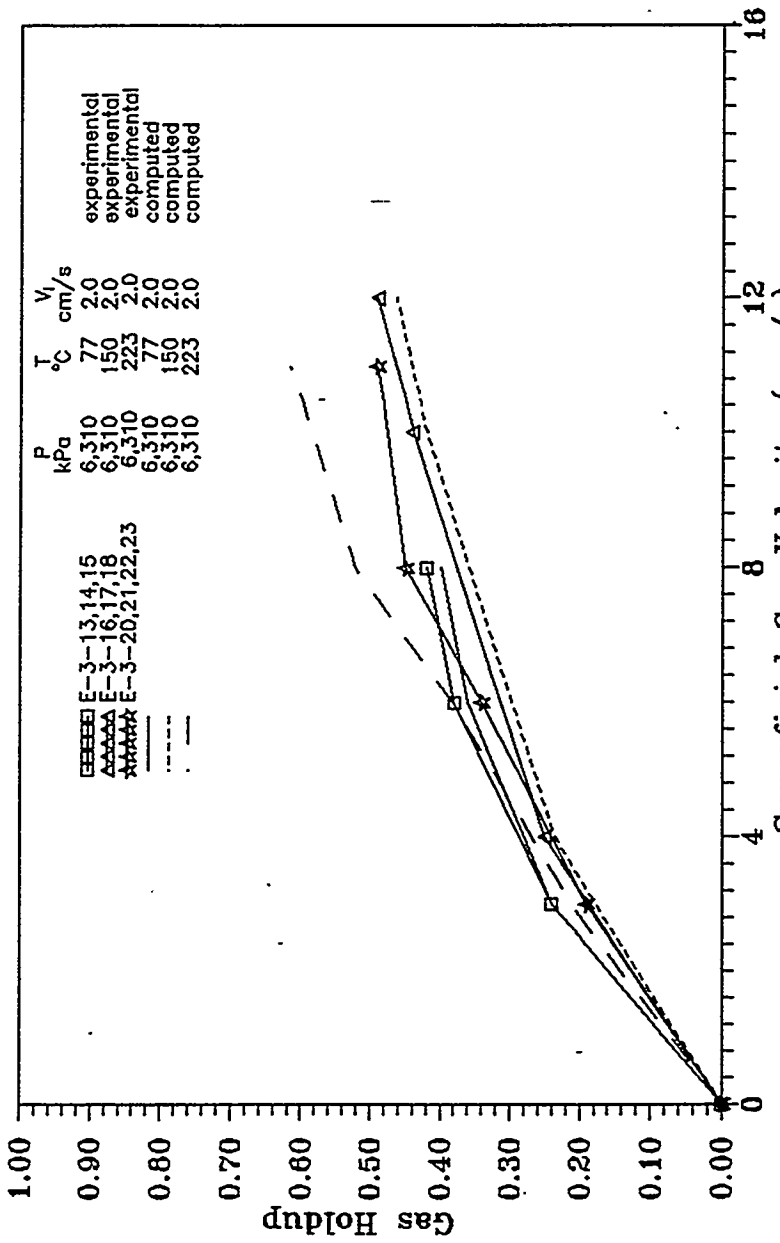

Figure 3.5 Effect of Temperature on Gas Holdup
(at Reactor Height=137cm)

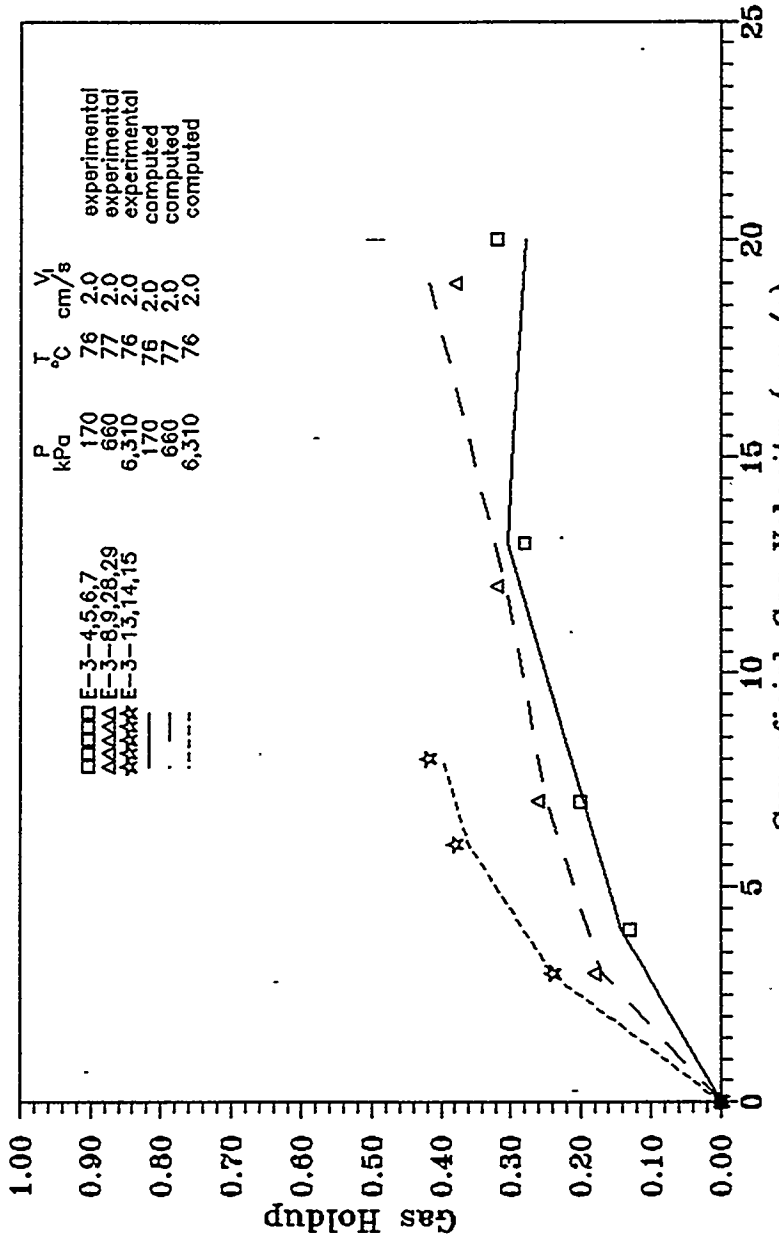

Figure 3.6 Effect of Pressure on Gas Holdup
(at Reactor Height=137cm)

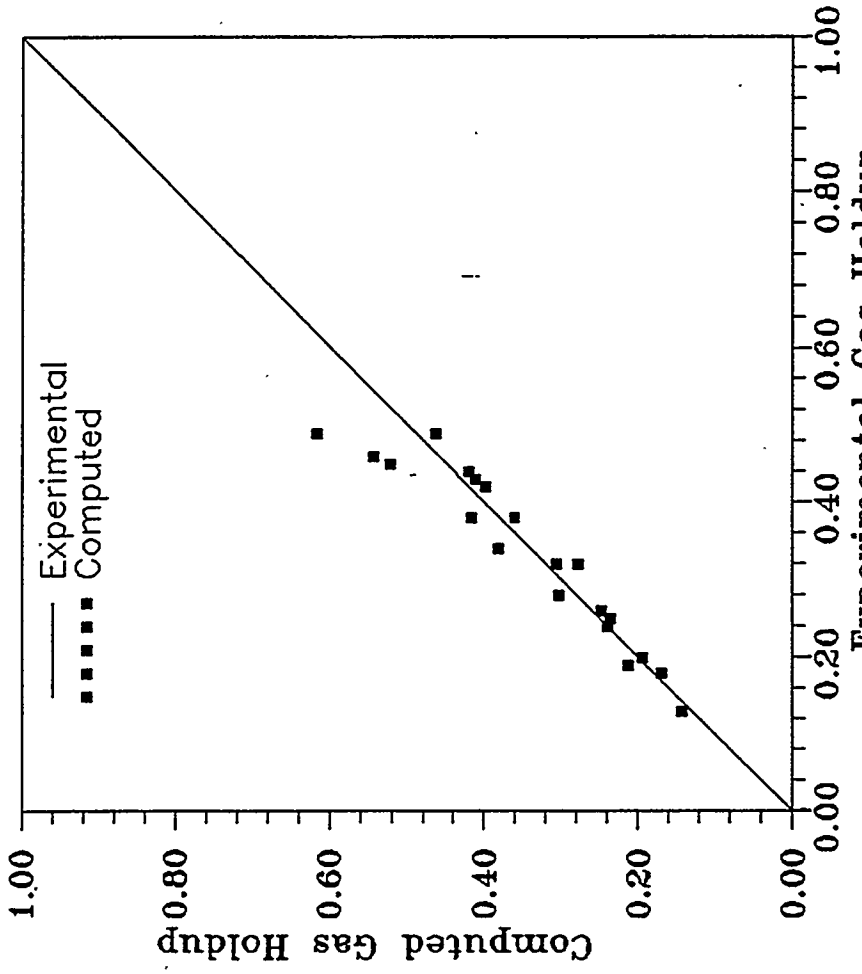

Figure 3.7 Comparison of Experimental and Computed Gas Holdup